Cellular and Molecular Life Sciences (2023) 80:99
https://doi.org/10.1007/s00018-023-04741-8

ORIGINAL ARTICLE

lncRNA miR4458HG modulates hepatocellular carcinoma progression by activating m6A-dependent glycolysis and promoting the polarization of tumor-associated macrophages

Ying Ye[1] · Menghan Wang[2] · Guoyu Wang[2] · Zhongchao Mai[2] · Borong Zhou[2] · Yang Han[2] · Juhua Zhuang[2] · Wei Xia[2]

Received: 10 October 2022 / Revised: 8 February 2023 / Accepted: 1 March 2023 / Published online: 18 March 2023

Abstract

Long non-coding RNAs (lncRNAs) play significant roles in different biological functions of cancers. However, their function in the metabolism of glucose in patients with human hepatocellular carcinoma (HCC) remains largely unknown. In this study, HCC and paired intact liver tissues were utilized to examine the miR4458HG expression using qRT-PCR and human HCC cell lines to examine cell proliferation, colony formation, and glycolysis after transfection of siRNAs targeting miR4458HG or miR4458HG vectors. The molecular mechanism of miR4458HG was clarified through in situ hybridization, Western blotting, qRT-PCR, RNA pull-down, and RNA immunoprecipitation analysis. The results showed that the miR4458HG affected HCC cell proliferation, activated the glycolysis pathway, and promoted the polarization of tumor-associated macrophage in vitro and in vivo models. Mechanistically, miR4458HG bound IGF2BP2 (a key RNA m6A reader) and facilitated IGF2BP2-mediated target mRNA stability, including HK2 and SLC2A1 (GLUT1), and consequently altered HCC glycolysis and tumor cell physiology. At the same time, HCC-derived miR4458HG could be wrapped in the exosomes and promoted the polarization of tumor-associated macrophage by increasing ARG1 expression. Hence, miR4458HG is oncogenic in nature among patients with HCC. To develop an effective treatment strategy of HCC patients presenting with high glucose metabolism, physicians should focus on miR4458HG and its pathway.

Keywords Long non-coding RNA · miR4458HG · Glycolysis · Hepatocellular carcinoma · IGF2BP2 · HK2 · GLUT1

Introduction

Hepatocellular carcinoma (HCC) ranks the sixth most common cancer worldwide and has a very poor prognosis [1]. To reduce deaths due to HCC, a noninvasive diagnostic tool is being developed for early identification of HCC or prediction of an individual's vulnerability [2]. However, there is a very little progression. HCC is characterized by a high metastatic rate, potential to invade, and aggressive angiogenetic ability, which are the primary challenges in the diagnosis and management of HCC [3]. Because the pathological mechanism of progression is not completely clear, further investigations are essential for finding and developing effective targets and biomarkers for the treatment and diagnosis of HCC.

The rearrangement of energy metabolism in cancer cells, especially the abnormal activation of glycolytic pathway, has been recognized as a marker of the initiation and malignancy of different cancers [4]. The cancer cells exhibit high glucose metabolism with enhanced lactic acid formation (major products of glycolysis pathway). These substances infiltrate the microenvironment, which reduces extracellular pH during glycolysis [5]. Lower levels of pH are closely correlated to poor prognosis of HCC in the microenvironment [6, 7] and increased cell proliferation and malignancy.

The lncRNAs are 200 bp in length that could affect different biological functions either without or a weak

Ying Ye and Menghan Wang Contributed equally.

✉ Wei Xia
tcm_xiawei@163.com

[1] Central Laboratory, The Seventh People's Hospital of Shanghai University of Traditional Chinese Medicine, Shanghai 200137, China

[2] Department of Nuclear Medicine, The Seventh People's Hospital, Shanghai University of Traditional Chinese Medicine, 358 Datong Rd, Pudong New Area, Shanghai 200137, China

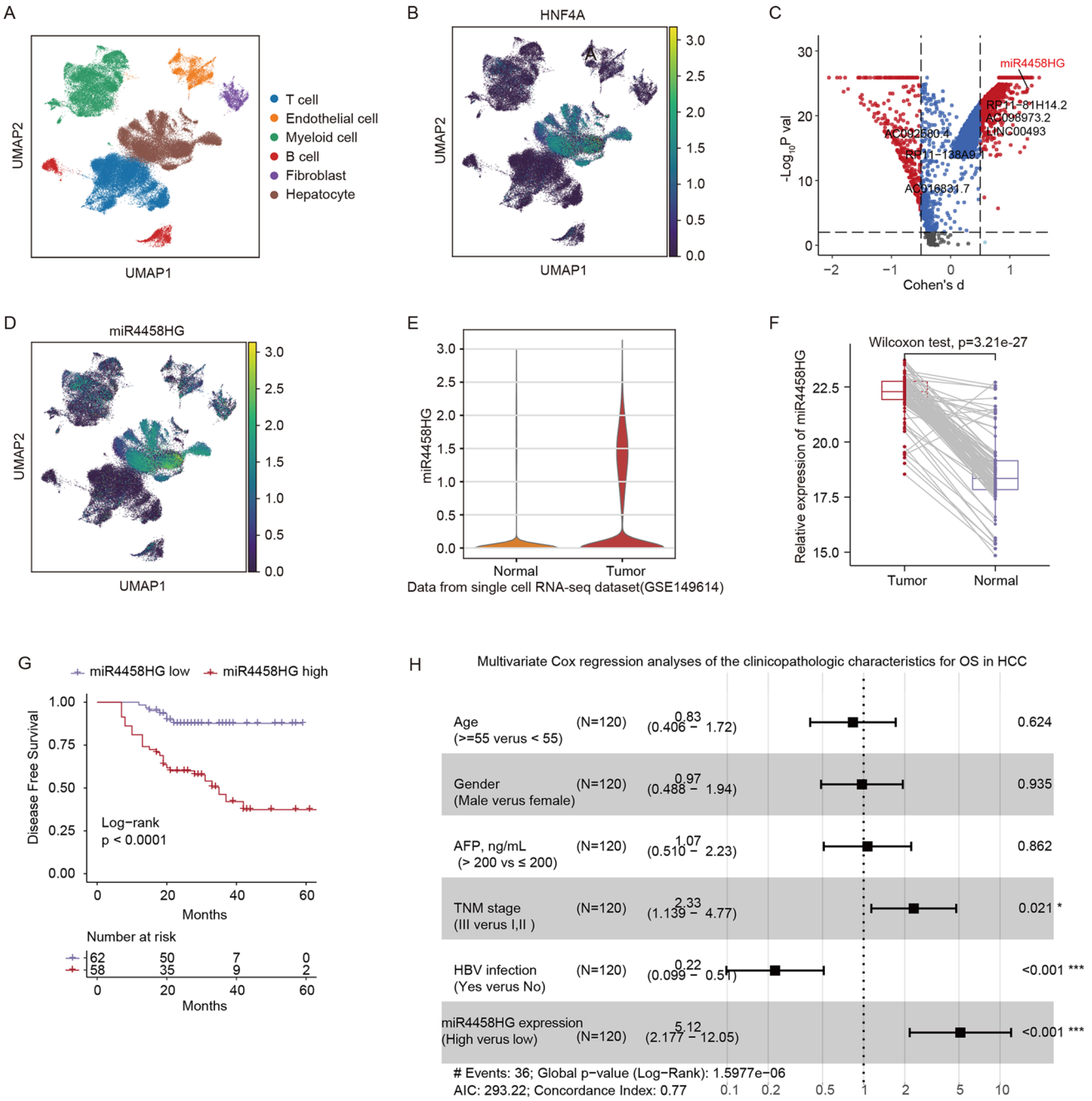

Fig. 1 miR4458HG lncRNA is clinically relevant in HCC. **A** UMAP plot of all cells colored by each cell type in HCC patients (GSE149614). **B** UMAP plot shows the expression of canonical marker genes for hepatocyte cells. **C** Volcano plot shows the differentially expressed genes between tumor cells and normal cells. The most significant expressed lncRNA miR4458HG is highlighted in red. **D** UMAP plot displays the expression of miR4458HG. **E** Violin plot shows the expression of miR4458HG in tumor cells and normal cells. **F** MiR4458HG expression in HCC tumor and the paired adjacent normal tissues of the cohort 1. **G** Survival analysis and comparison among people with greater and lesser values of miR4458HG expression in tumor in cohort 1; $n = 120$, log-rank test. **H** Multivariate Cox analysis of miR4458HG expression and clinicopathological variables

protein-coding ability [8]. lncRNAs can influence cancer initiation and development [9, 10]. These include HOTAIR, MEG3, and MALAT-1 and play roles in various carcinogenesis [11, 12]. However, the specific mechanism of lncRNA in HCC initiation and glucose metabolism remains to be further studied.

Hence, in this study, we aimed to investigate the gene expression, clinical importance, function, and possible

mechanism of action of the novel lncRNA in HCC patients. Single-cell RNA-seq data from GSE149614 database and TCGA HCC bulk-RNA sequencing data were used to examine the expression of genome-wide lncRNA. MiR4458HG is lncRNA highly expressed among HCC patients and correlated with poor prognosis and glycolysis. Mechanistically, miR4458HG regulated the m6A modification and mRNA stability of *SLC2A1* and *HK2* by promoting the binding efficiency of IGF2BP2 to the m6A motif in these two genes, which are the crucial limiting enzyme and glucose transporter for the catalysis of glycolysis. MiR4458HG, HK2, and GLUT1 are associated with some malignant pathophysiological features that result in clinically poor prognosis of HCC. In addition, HCC-derived miR4458HG could be wrapped in the exosomes and regulate the polarization of tumor-associated macrophage in the tumor microenvironment. Thus, miR4458HG-IGF2BP2-*HK2*/*SLC2A1* (GLUT1) as a cascade reaction may offer innovative and promising treatment options for HCC.

Materials and methods

Clinical samples

Resected tumor was collected along with some normal tissue attached to the affected tissues in HCC patients who preferred surgery at The Seventh People's Hospital of Shanghai University of Traditional Chinese Medicine. The research was approved by institutional Ethics Committee, at The Seventh People's Hospital of Shanghai University of Traditional Chinese Medicine, and informed consents were received.

HCC cell lines and culture conditions

Hep3B, BEL-7402, Huh7, and SMMC-7721 cell lines were purchased from the American Type Culture Collection. All cell lines were cultured in the suggested growth medium augmented with 10% fetal bovine serum and incubated at 37 °C under 5% CO_2. In a 12-well Transwell system, HCC cancer cells were added to the lower chamber, while monocyte-derived macrophages (MDMs) were added to the upper chamber. The pore size of the upper chamber was 0.4 µm. After a co-culture for 10 days, the macrophages were removed, and the HCC cells were washed once with phosphate buffered saline and cultured in fresh medium.

Bioinformatics analysis

The raw gene counts of HCC were obtained from GEO source (https://www.ncbi.nlm.nih.gov/geo/query/acc.cgi?acc=GSE149614). The unique molecular identifier value was changed in to anndata objects (version 0.6.22) by a Scanpy package v1.4.4. UMAP was utilized for identification. Annotated cell types that evolved from the expression of known marker genes were used. Effect size was evaluated using Cohen's *d* statistics to estimate the magnitude of differentially expressed gene between normal cells and tumor cells.

Plasmids and adenovirus renderings

The control pcDNA3.1 plasmid, miR4458HG overexpression plasmid, SLC2A1 overexpression plasmid, and HK2 overexpression plasmid were created by Generay Technologies (Shanghai, China). The control pShuttle-H1 shRNA adenovirus, miR4458HG shRNA adenovirus, control pShuttle-CMV adenovirus, SLC2A1 overexpression adenovirus, and HK2 overexpression adenovirus were formulated by Obio Technology Company (Shanghai, China). All these information on the shRNAs are listed in Table S1.

Plasmids or siRNA transfection

The samples were infected with pcDNA3.1, pShuttle-CMV or pShuttle-H1 plasmids using FuGENE HD transfection reagent (Promega). Small interfering RNAs (Shanghai GenePharma Co., Ltd) were added into the HCC cells by DharmaFECT 1 siRNA infection reagent (Thermo Fisher Scientific). Empty vector and non-specific siRNA were utilized as negative controls. Complete sequences of siRNAs are listed in Table S1.

Generation of miR4458HG-knockout BEL-7404 cells (ΔmiR4458HG)

Lentiviral-based CRISPR gene editing system (LentiCRISPR) was used to establish miR4458HG-knockout BEL-7404 cells. Genome engineering experiments utilizing CRISPR-Cas9 systems was conducted as previously described [13].

Cell proliferation and colony formation assay

Cell proliferation was analyzed by Cell Counting Kit-8 (Dojindo, Japan). Briefly, control or transfected HCC samples were planted into 96-well culture plates with a primary density of 3×10^3 cells per well. At the specified time points, Cell Counting Kit-8 was installed into the cells. Then the cells were incubated for 2 h at 37 °C, and the absorbance was recorded based on the manufacturer's directions.

For the colony formation assay, cells were transfected with indicated plasmid or siRNA. A total of 600 treated cells were placed in the 6-well culture plates. After 7–10 days of culture, the cells were fixed with 4% paraformaldehyde,

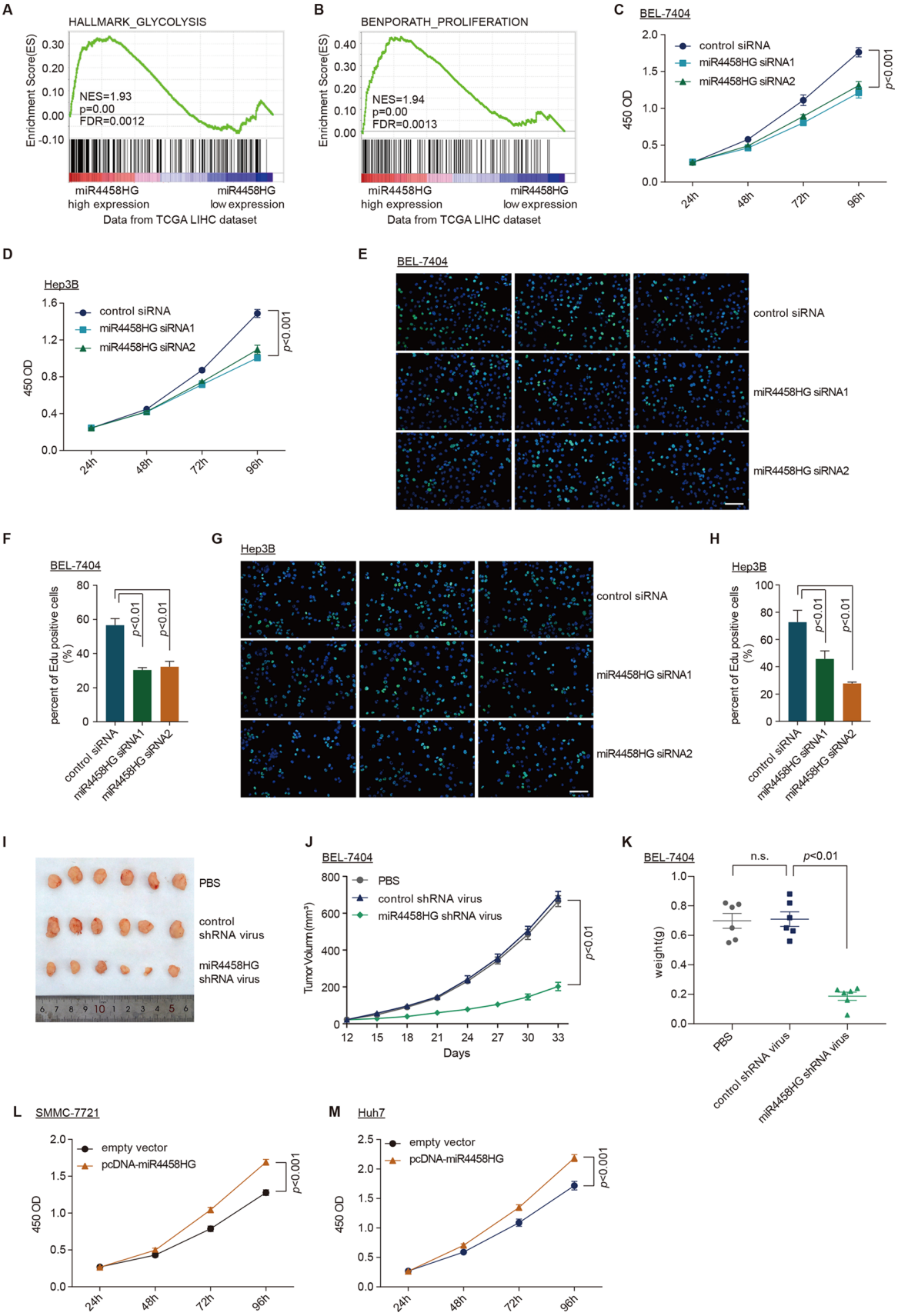
A
HALLMARK_GLYCOLYSIS
Enrichment Score(ES)
NES=1.93
p=0.00
FDR=0.0012
miR4458HG high expression
miR4458HG low expression
Data from TCGA LIHC dataset
B
BENPORATH_PROLIFERATION
NES=1.94
p=0.00
FDR=0.0013
C
BEL-7404
control siRNA
miR4458HG siRNA1
miR4458HG siRNA2
450 OD
p<0.001
D
Hep3B
E
BEL-7404
F
BEL-7404
percent of Edu positive cells (%)
p<0.01
G
Hep3B
H
Hep3B
I
PBS
control shRNA virus
miR4458HG shRNA virus
J
BEL-7404
Tumor Valumn (mm³)
Days
K
BEL-7404
n.s.
p<0.01
weight(g)
L
SMMC-7721
empty vector
pcDNA-miR4458HG
M
Huh7

◂**Fig. 2** miR4458HG is a carcinogenic lncRNA in HCC. **A**, **B** GSEA data showed the enrichment of GLYCOLYSIS (**A**) and BENPORATH_PROLIFERATION (**B**) peaks in subjects with high miR4458HG expression compared with low miR4458HG expression. NES, normalized enrichment score; FDR, false discovery rate. **C**, **D** Cell proliferation assay was performed in BEL-7404 and Hep3B cells transfected with miR4458HG siRNA. **E**, **F** EdU assay was performed in BEL-7404 cells transfected with miR4458HG siRNA (**E**). Scale bar, 100 μm. The quantification of EdU staining (**F**). **G**, **H** EdU assay was performed in Hep3B cells transfected with miR4458HG siRNA (**G**). Scale bar, 100 μm. The quantification of EdU** staining (**H**). **I** Sample images of tumor among mice bearing BEL-7404 cells treated using different treatment. **J** Tumor volume was evaluated after miR4458HG shRNA adenovirus treatments in the xenograft mouse model ($n=6$). **K** Weight of tumor quantified in mice following different treatments ($n=6$). **L**, **M** Cell proliferation assay was performed in SMMC-7721 and Huh7 cells infected using pcDNA3.1-miR4458HG

stained with 0.1% crystal violet, that was washed using dH_2O and then dried.

EdU assay

The proliferation ability of HCC cells was detected using EdU assay. In brief, the cells were seeded into 24-well plates and transfected with indicated siRNA for 24 h. Subsequently, the cells were incubated with EdU solution for 2 h, washed with PBS for three times, fixed with 4% paraformaldehyde, and neutralized with glycine, reacted with Alexa fluorescent dyes. Finally, DAPI was used to stain the nuclei. The results were observed using an inverted fluorescence microscope (Olympus, Tokyo, Japan). The proportion of EdU positively stained cells (green fluorescence) to DAPI-stained cells (blue fluorescence) was calculated. The results were analyzed using image J version 1.52 software.

RNA extraction and quantitative real-time PCR (qRT-PCR)

Total RNAs were eliminated from HCC tissues or cell lines using TRIzol reagent (Invitrogen), and 1 μg of the total RNAs was reverse transcribed to synthesize cDNA utilizing PrimeScript RT Reagent Kit (Takara). qRT-PCR was performed using Power SYBR Green PCR Master Mix (Thermo). β-Actin was used as the internal control. Primer sequences are listed in Table S2.

Western blot

HCC cells were collected and lysed on ice by lysis buffer (50 mM Tris–HCl [pH 8.0], 150 mM NaCl, 1% NP-40 and 0.5% sodium deoxycholate, complete protease inhibitor cocktail [Roche Applied Science]) and quantified by BCA Protein Assay Kit (Beyotime Biotechnology). Subsequently, 40 μg protein was isolated by SDS–polyacrylamide gels and then shifted to PVDF membranes (Millipore). The membranes were masked with 5% non-fat milk for 1 h and incubated with primary antibody anti-IGF2BP2 (Abcam; ab124930), anti-HK2 (Abcam; ab209847), anti-GLUT1 (Abcam; ab115730), anti-RBMX (Abcam; ab244514), anti-CLK1 (Abcam; ab74044), anti-UTP6 (Abnova; H00055813-K), anti-GIT1 (Abnova; PAB20257), and anti-GAPDH (Abcam; ab9485) at room temperature for 1 h. Secondary antibodies were labeled with HRP. Visualization was performed using an ECL detection system (Bio-Rad).

Immunohistochemistry and in situ hybridization (ISH)

Immunohistochemistry was conducted based on the standard protocols. In brief, HCC tissue was dissected and attached with 4% PFA for a night at 4 °C prior to placement in paraffin. Paraffin-embedded sections were rehydrated, and heat-mediated antigen retrieval was carried out by microwave with sodium citrate. At room temperature, the sections were incubated in a blocking solution for 2 h. Then the sections were incubated with indicated antibodies on a humidified box for 24 h at 4 °C. These sections were cleansed and incubated with secondary antibody. For the color reaction, DAB substrate kit was utilized, and for nucleus counterstaining, hematoxylin was preferred. The expression of miR4458HG in HCC was evaluated by biotin-labeled miR4458HG ISH probes (BOSTER, Wuhan, China) in line with manufacturer's directions.

In vivo tumor formation

BEL-7404 cells or BEL-7404 miR4458HG-KO cells were infused in the right flank of randomly selected 4-week-old male BALB/c mice (Model Animal Research Center of Nanjing University, Nanjing, China). The organization, development, and size of the tumor were documented every 3 days. Seven days after immunization, the mice were infused with adenovirus by multipoint intra-tumoral injection once in every 2 days. Five weeks later, the experimental subjects were sacrificed to extract the xenograft tumors for measurement and analysis. Tumor volume (mm^3) was calculated: Tumor volume (mm^3) = longer diameter × shorter diameter^2/2. The animal research was approved by the Animal Care and Use Committee of The Seventh People's Hospital of Shanghai University of Traditional Chinese Medicine.

RNA immunoprecipitation

RNA immunoprecipitation (RIP) experiments were performed using the Megna RIP Kit (Millipore). RNA immunoprecipitation lysis buffer was used for cell preparation,

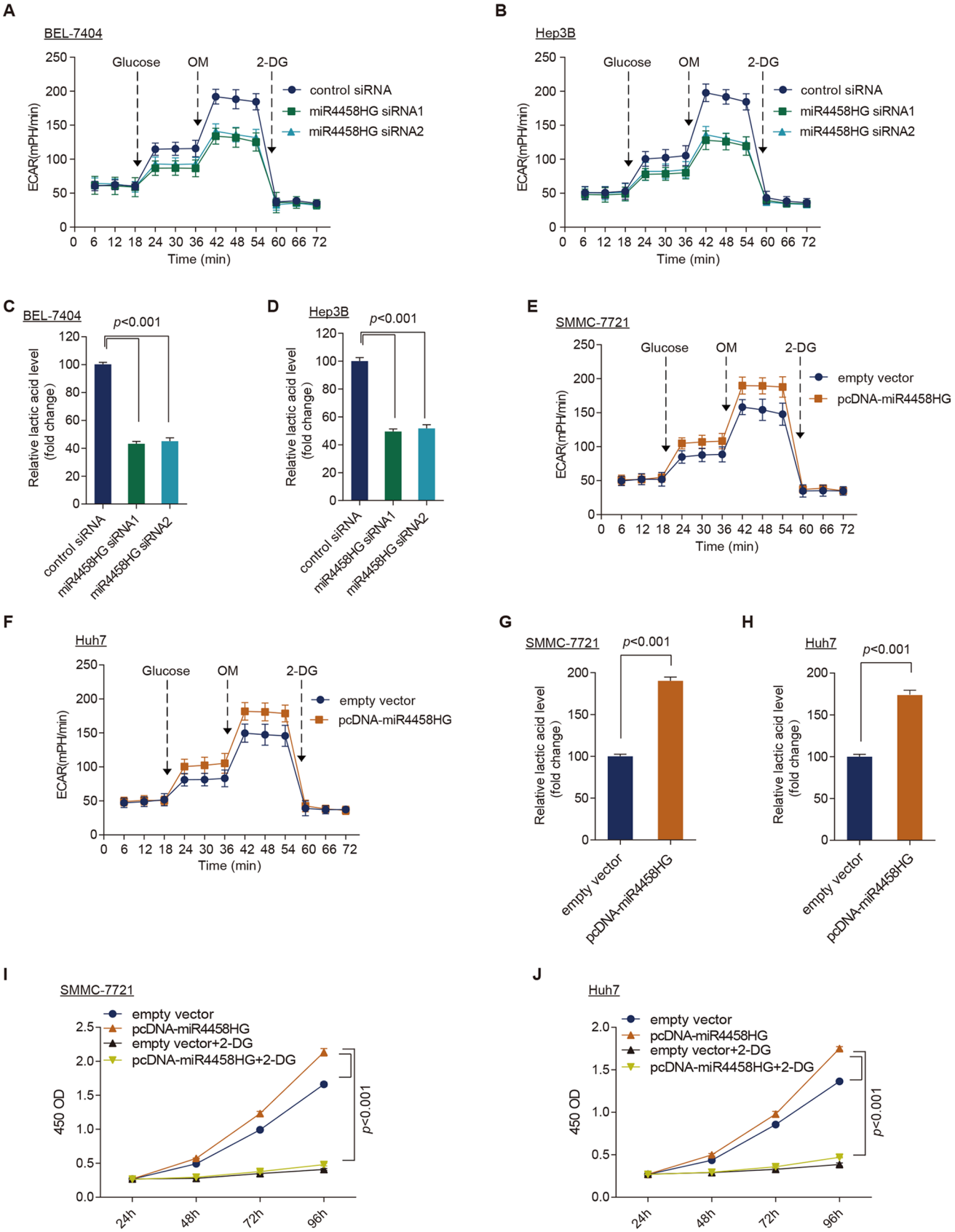
A
BEL-7404
Glucose
OM
2-DG
control siRNA
miR4458HG siRNA1
miR4458HG siRNA2
ECAR(mPH/min)
Time (min)
B
Hep3B
C
BEL-7404
p<0.001
Relative lactic acid level (fold change)
D
Hep3B
E
SMMC-7721
empty vector
pcDNA-miR4458HG
F
Huh7
G
SMMC-7721
H
Huh7
I
SMMC-7721
empty vector+2-DG
pcDNA-miR4458HG+2-DG
450 OD
24h
48h
72h
96h
J
Huh7

◂**Fig. 3** miR4458HG-influenced cell longevity is determined by glycolytic metabolism. **A**, **B** ECAR was detected in BEL-7404 (**A**) and Hep3B (**B**) cells transfected with control or miR4458HG siRNA. *OM* oligomycin, *2-DG* 2-deoxyglucose. **C**, **D** Lactic acid production was measured in BEL-7404 (**C**) and Hep3B (**D**) cells with control or miR4458HG siRNA transfection. **E**, **F** ECAR was quantified after transfecting with control or pcDNA3.1-miR4458HG in SMMC-7721 (**E**) and Huh7 (**F**) cells. **G**, **H** Lactic acid production was measured in SMMC-7721 (**G**) and Huh7 (**H**) cells with control or pcDNA3.1-miR4458HG transfection. **I**, **J** Cell proliferation was performed in SMMC-7721 (**I**) and Huh7 (**J**) cells after transfection with control or pcDNA3.1-miR4458HG, and followed by 5 mM 2-DG treatment

and the RNA–protein complexes were immunoprecipitated using anti-IGF2BP2 antibody (Abcam; ab124930) and rabbit IgG as the negative control. The co-precipitated RNAs were detected by qRT-PCR.

HCC cells transfected with miR-100-3p or miR-NC were collected 48 h post-transfection to conduct the RIP experiments. The RNA–protein complexes were immunoprecipitated using an AGO2 antibody (Abcam; ab186733). The RNA fraction separated by RIP was analyzed by qRT-PCR.

RNA stability assay

Actinomycin D was used to treat HCC cells with or without miR4458HG knockdown at 0, 3, and 6 h at a final concentration of 5 μg/mL. Total RNAs were removed, and qRT-PCR was performed to measure the relative mRNA values of SLC2A1 or HK2.

Measurement of extracellular acidification rate

The extracellular acidification rate (ECAR) was measured with the seahorse XF glycolysis stress test kit (Agilent Technologies) and analyzed by the seahorse extracellular Flux analyzer XF96 (Seahorse Bioscience) as per the manufacturer's directions. The cells were transfected with control siRNA, miR4458HG siRNA, control plasmid, or miR4458HG overexpression plasmid and inserted into the 96-well cell culture plates and incubated at 37 °C overnight. Afterward, the cells were used to measure ECAR. After measurement of baseline concentration, glucose, oligomycin, and 2-deoxyglucose (2-DG) were added one by one into each well for ECAR measurement.

Lactate production analysis

L-Lactate Assay Kit (Colorimetric [Abcam]) was preferred in quantifying the lactate production as per the manufacturer's directions. The transfected cells were seeded into six-well plates and subsequently they were incubated at 37 °C overnight. Following a starvation period of 2 h, the culture medium was collected to quantify the lactate formation at 450 nm in a microplate reader. The results were normalized to the total protein strength of every sample.

RNA pull-down assay

Similar numbers of cell lysates along with biotin-labeled anti-sense RNA, full-length sense RNA, and truncated RNA were incubated with streptavidin beads. Following the pull-down, the interacted proteins were eluted with 1 × SDS loading buffer. Proteins that interacted were isolated by SDS-PAGE gel and then shifted to the PVDF membrane. The IGF2BP2 antibody was used in the Western blot analysis.

Chromatin isolation by RNA purification (ChIRP)

HCC cells were collected and isolated using chromatin by RNA purification (ChIRP) experiments. The RNA–RNA complexes were immunoprecipitated using biotin-labeled miR4458HG anti-sense RNA or control RNA. The RNA fraction separated by ChIRP was analyzed by qRT-PCR. The pull-down efficiency of miR4458HG was analyzed by qRT-PCR, with 18S RNA as negative control. The miR-100-3p level was analyzed by qRT-PCR and U6 was used as negative control.

Cytoplasmic and nuclear fraction

Cells were washed once with cold PBS and pelleted by centrifugation. To collect the cytoplasmic fraction, the pellet was then resuspended in five pellet volumes of hypotonic lysis buffer (10 mM Tris [pH 7.5], 10 mM NaCl, 3 mM MgCl2, 0.3% [vol/vol] NP-40, 10% [vol/vol] glycerol). Cytoplasmic RNA was obtained by ethanol precipitation followed by re-extraction using a TRIzol reagent. The remaining nuclear pellet was washed three times with the hypotonic lysis buffer, followed by extraction with TRIzol reagent according to the manufacturer's instructions.

Liquid chromatography–mass spectrometry (LC–MS) analysis

LC–MS was performed as previously described [14]. Briefly, cells were labeled with SILAC medium (DMEM containing Leu-d3). The lighter (in normal medium) and heavy (in Leu-d3 medium) cells were collected and lysed. The number of proteins extracted from heavy and light cells were equal. The proteins were incubated with biotin-labeled anti-sense RNA and sense RNA, and then with streptavidin beads. After RNA pull-down, the beads belonging to two fractions were combined and proteins were eluted by 1 × SDS loading buffer. 12% SDS-PAGE gel and stained with Coomassie brilliant blue were used.

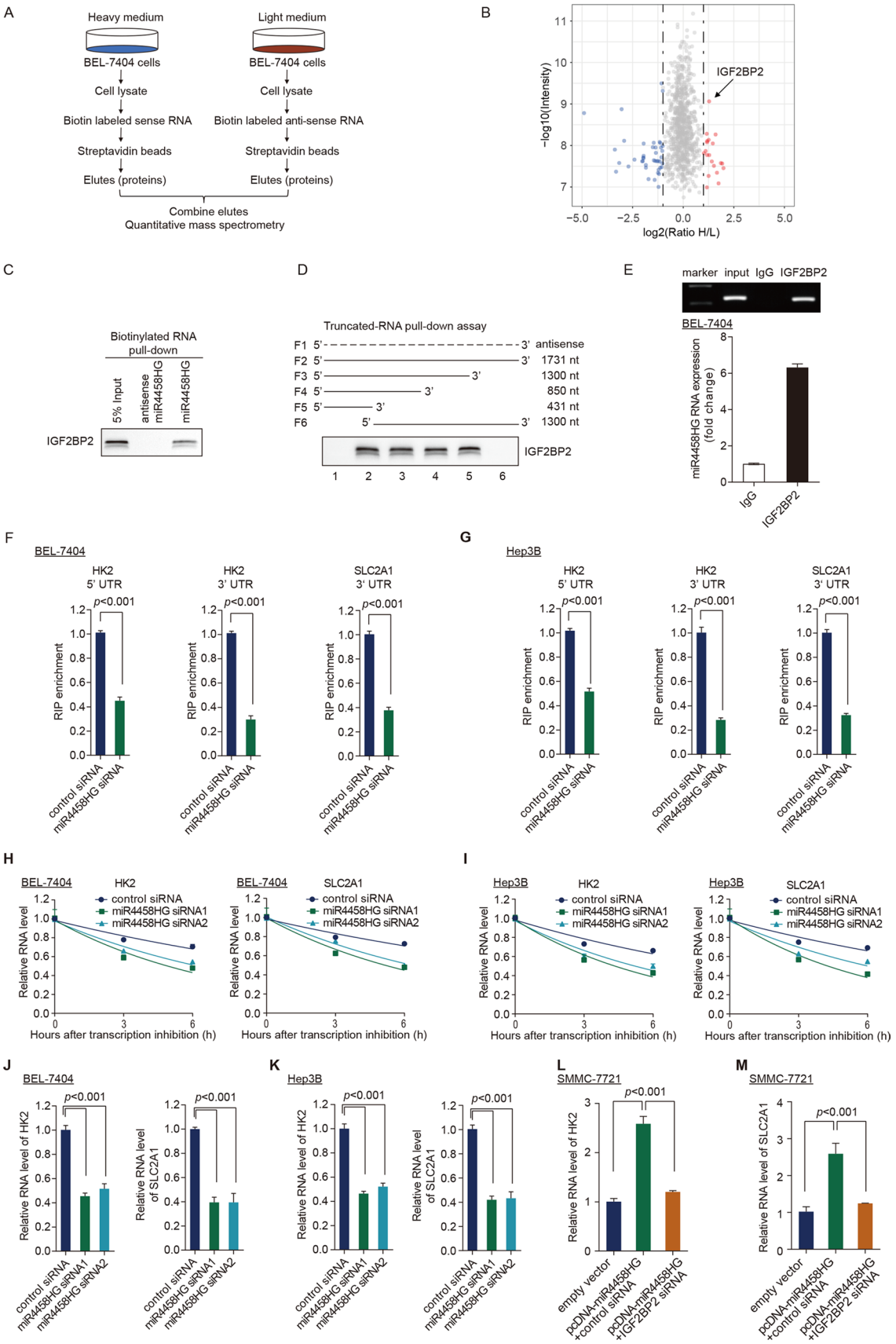
A
Heavy medium
Light medium
BEL-7404 cells
BEL-7404 cells
Cell lysate
Cell lysate
Biotin labeled sense RNA
Biotin labeled anti-sense RNA
Streptavidin beads
Streptavidin beads
Elutes (proteins)
Elutes (proteins)
Combine elutes
Quantitative mass spectrometry
B
IGF2BP2
−log10(Intensity)
log2(Ratio H/L)
C
Biotinylated RNA pull-down
5% Input
antisense miR4458HG
miR4458HG
IGF2BP2
D
Truncated-RNA pull-down assay
F1 5' 3' antisense
F2 5' 3' 1731 nt
F3 5' 3' 1300 nt
F4 5' 3' 850 nt
F5 5' 3' 431 nt
F6 5' 3' 1300 nt
IGF2BP2
1 2 3 4 5 6
E
marker input IgG IGF2BP2
BEL-7404
miR4458HG RNA expression (fold change)
IgG
IGF2BP2
F
BEL-7404
HK2 5' UTR
HK2 3' UTR
SLC2A1 3' UTR
p<0.001
RIP enrichment
control siRNA
miR4458HG siRNA
G
Hep3B
HK2 5' UTR
HK2 3' UTR
SLC2A1 3' UTR
p<0.001
RIP enrichment
control siRNA
miR4458HG siRNA
H
BEL-7404 HK2
BEL-7404 SLC2A1
control siRNA
miR4458HG siRNA1
miR4458HG siRNA2
Relative RNA level
Hours after transcription inhibition (h)
I
Hep3B HK2
Hep3B SLC2A1
control siRNA
miR4458HG siRNA1
miR4458HG siRNA2
Relative RNA level
Hours after transcription inhibition (h)
J
BEL-7404
p<0.001
Relative RNA level of HK2
Relative RNA level of SLC2A1
control siRNA
miR4458HG siRNA1
miR4458HG siRNA2
K
Hep3B
p<0.001
Relative RNA level of HK2
Relative RNA level of SLC2A1
control siRNA
miR4458HG siRNA1
miR4458HG siRNA2
L
SMMC-7721
p<0.001
Relative RNA level of HK2
empty vector
pcDNA-miR4458HG +control siRNA
pcDNA-miR4458HG +IGF2BP2 siRNA
M
SMMC-7721
p<0.001
Relative RNA level of SLC2A1
empty vector
pcDNA-miR4458HG +control siRNA
pcDNA-miR4458HG +IGF2BP2 siRNA

◂**Fig. 4** miR4458HG reacts with IGF2BP2 and regulates the stability of SLC2A1 and HK2. **A** Schematic representation of SILAC-based quantitative proteomic method to identify the miR4458HG-specific interactors. **B** Proteome-wide accurate measure showed statistical significance. **C** Western blot analysis of IGF2BP2 from miR4458HG and anti-sense miR4458HG pull-down assay. **D** Western blot analysis of IGF2BP2 in samples pulled down by anti-sense (F1), full-length (F2), or truncated miR4458HG (F3: 1–1300, F4: 1–850, F5: 1–431, F6: 432–1731). **E** RNA immunoprecipitation was performed using IGF2BP2 antibody, and specific primer was used to measure miR4458HG. **F**, **G** RIP-PCR showed the binding enrichment of IGF2BP2 to HK2 and SLC2A1 (GLUT1) was diminished with the knockdown of miR4458HG in BEL-7404 cells (**F**) and Hep3B cells (**G**). **H**, **I** The half-life of HK2 and SLC2A1 mRNA was measured by qRT-PCR in BEL-7404 cells (**H**) and Hep3B cells (**I**) with control or miR4458HG siRNA transfection. **J**, **K** The HK2 and SLC2A1 mRNA were detected by qRT-PCR in BEL-7404 cells (**J**) and Hep3B cells (**K**) with control or miR4458HG siRNA transfection. **L** The relative HK2 expression level in SMMC7721 cells transfected with pcDNA-miR4458HG and indicated siRNAs. **M** The relative SLC2A1 expression level in SMMC7721 cells transfected with pcDNA-miR4458HG and indicated siRNAs

Exosome experiment

Exosomes were separated from the cell culture medium by ultracentrifugation. The medium was centrifuged at 1,000 g for 10 min at 4 °C. Next, to remove the cellular debris, the supernatant was centrifuged at 10,000*g* for 30 min at 4 °C. The resulting supernatant was then passed through a 0.22-μm filter and then subjected to ultracentrifugation at 100,000*g* at 4 °C for 90 min. The resulting pellet contained the exosomes.

The purity of the exosome was examined by electron microscopy. Primary antibodies against CD9, CD81, and Alix were used to identify the exosomes.

Equal numbers of exosomes derived from the Hep3B cells were treated with RNaseA and TritonX-100. RNA was then extracted with TRIzol and normalized to cel-39-3p for qRT-PCR.

For the visualization of lncRNA and exosome co-localization, FAM-labeled miR4458HG (in vitro transcription) were introduced into the exosomes by electroporation. The exosomes were labeled with Dil (LMAI Bio.). MDMs were incubated with Dil-labeled exosomes and visualized by laser scanning confocal microscopy (TCS SP8, Leica).

Luciferase reporter assay

pGLO, pGLO-miR4458HG, or pGLO-miR4458HG mut (miR-100-3p binding site), pGLO-ARG1, or pGLO-ARG1 mut (miR-100-3p binding site) was co-transfected with miR-100-3p mimics or miR-Control in MDMs. The relative luciferase activity was normalized to Renilla luciferase activity. Firefly luciferase activity and Renilla luciferase activity were measured using a dual-luciferase reporter assay system (Promega) according to the manufacturer's protocol.

Quantification and statistical analysis

The results were interpreted using Mann–Whitney *U* test in GraphPad Prism. Data are presented as mean ± SEM. p values < 0.05 were considered statistically significant.

Results

miR4458HG lncRNA is clinically relevant in HCC

Recent evidence suggest that lncRNAs play important roles in the initiation and progression of HCC. We re-analyzed the single-cell RNA-seq data from GSE149614. Totally, 34,414 cells derived from HCC tumor tissues ($n = 10$) and 28,687 cells from adjacent normal tissues ($n = 8$) were analyzed. These cells were annotated by marker genes as six cell types, hepatocyte, T cells, B cells, myeloid cells, endothelial cells, and fibroblast according to the original study [15] (Figs. 1A, S1A). To investigate the lncRNA specifically expressed in the HCC tumor tissue, the hepatocyte cells ($n = 22{,}461$) were extracted from the single-cell dataset (Fig. 1B). To determine whether the lncRNAs exert differential effects on HCC tumorigenesis, the scRNA-seq transcriptome of each hepatocyte cell was compared between the tumor tissue and the normal tissue. Among the differentially expressed transcripts, the miR4458HG was most significantly expressed in the tumor tissue with a large effect size (|Cohens' d|> 0.1 and $p < 0.01$) (Fig. 1C). Uniform Manifold Approximation and Projection (UMAP) analysis shows that the lncRNA miR4458HG was mainly enriched in hepatocyte cell (Fig. 1D), especially in HCC cell (Fig. 1E). Further, in 120 HCC patients (cohort 1 of hospital), the expression of the lncRNA miR4458HG was significantly higher in the tumor tissue than in the normal tissue (Fig. 1F). This result was confirmed by TCGA HCC dataset (TCGA LIHC) (Fig. S1B). Further, we analyzed the correlation among miR4458HG expression level and different clinical presentations of pathophysiology of HCC in hospital cohort 1 (Table S3). Results of the survival analysis revealed that the HCC patients with a higher miR4458HG expression had a short relapse time in the TCGA cohort ($p = 0.019$, HR 1.4) (Fig. S1C) and hospital cohort 1 (Fig. 1G). Based on the multivariable Cox regression, lncRNA miIR4458HG is independently associated with the survival time of HCC in TCGA cohort (Fig. 1H).

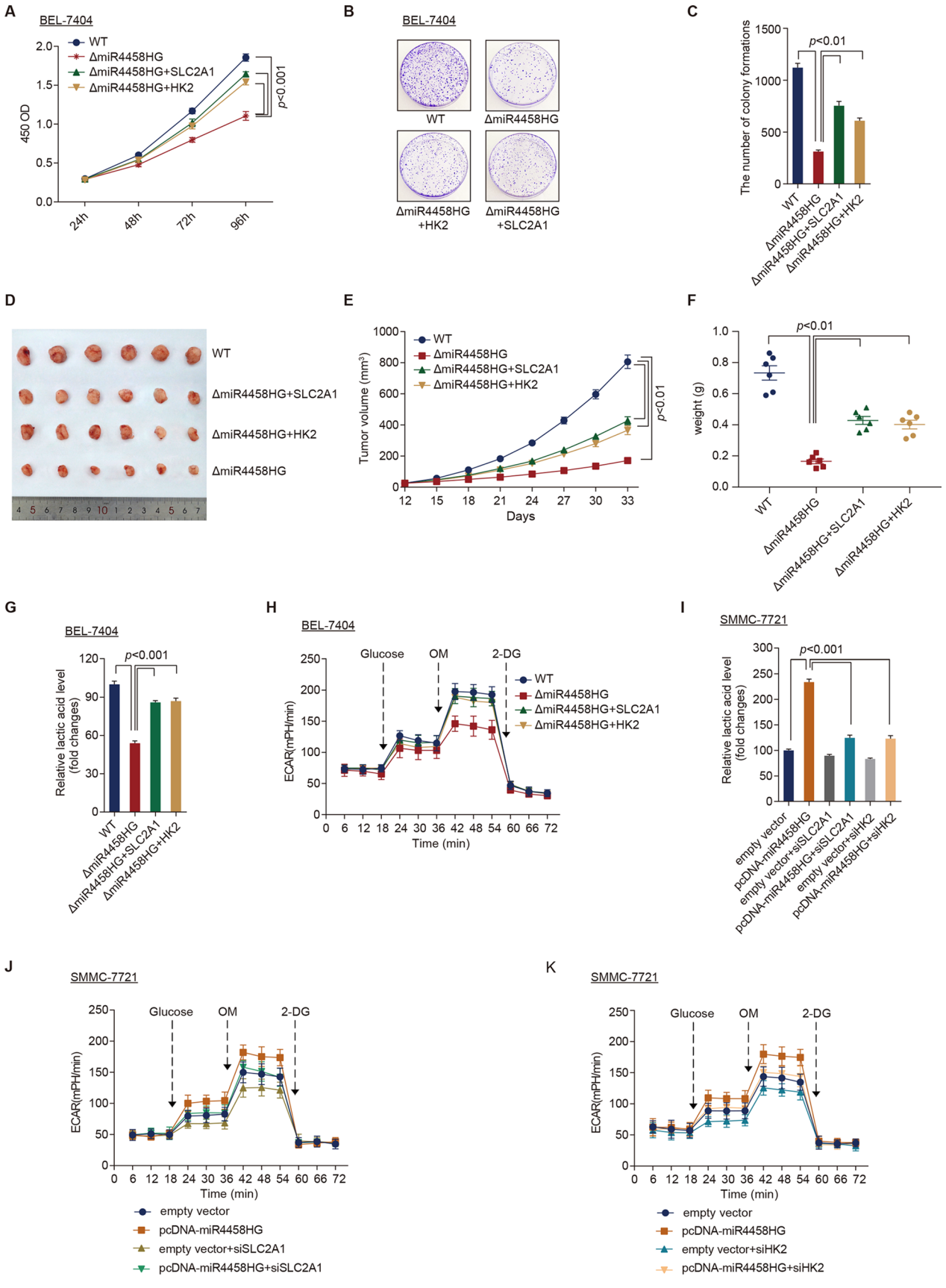
A
BEL-7404
WT
ΔmiR4458HG
ΔmiR4458HG+SLC2A1
ΔmiR4458HG+HK2
450 OD
p<0.001
24h
48h
72h
96h
B
BEL-7404
WT
ΔmiR4458HG
ΔmiR4458HG +HK2
ΔmiR4458HG +SLC2A1
C
The number of colony formations
p<0.01
WT
ΔmiR4458HG
ΔmiR4458HG+SLC2A1
ΔmiR4458HG+HK2
D
WT
ΔmiR4458HG+SLC2A1
ΔmiR4458HG+HK2
ΔmiR4458HG
E
Tumor volume (mm³)
WT
ΔmiR4458HG
ΔmiR4458HG+SLC2A1
ΔmiR4458HG+HK2
p<0.01
Days
F
weight (g)
p<0.01
WT
ΔmiR4458HG
ΔmiR4458HG+SLC2A1
ΔmiR4458HG+HK2
G
BEL-7404
Relative lactic acid level (fold changes)
p<0.001
WT
ΔmiR4458HG
ΔmiR4458HG+SLC2A1
ΔmiR4458HG+HK2
H
BEL-7404
Glucose
OM
2-DG
ECAR(mPH/min)
WT
ΔmiR4458HG
ΔmiR4458HG+SLC2A1
ΔmiR4458HG+HK2
Time (min)
I
SMMC-7721
Relative lactic acid level (fold changes)
p<0.001
empty vector
pcDNA-miR4458HG
empty vector+siSLC2A1
pcDNA-miR4458HG+siSLC2A1
empty vector+siHK2
pcDNA-miR4458HG+siHK2
J
SMMC-7721
Glucose
OM
2-DG
ECAR(mPH/min)
Time (min)
empty vector
pcDNA-miR4458HG
empty vector+siSLC2A1
pcDNA-miR4458HG+siSLC2A1
K
SMMC-7721
Glucose
OM
2-DG
ECAR(mPH/min)
Time (min)
empty vector
pcDNA-miR4458HG
empty vector+siHK2
pcDNA-miR4458HG+siHK2

◂**Fig. 5** HK2 and SLC2A1 were functionally significant target genes of miR4458HG in HCC. **A** Cell proliferation was performed after the overexpression of SLC2A1 and HK2 in BEL-7404 miR4458HG-knockout cells. **B**, **C** Colony formation assay was measured after overexpression of SLC2A1 and HK2 in BEL-7404 miR4458HG-knockout cells. **D** Sample picture of tumors in mice bearing BEL-7404 WT and miR4458HG-knockout cells treated with control adenovirus, SLC2A1 overexpression adenovirus or HK2 overexpression adenovirus ($n=6$). **E** Volume of the tumor was quantified after different treatments in the xenograft mouse model ($n=6$). **F** Tumor weight of mice was measured following respective treatments ($n=6$). **G** Lactic acid production was examined in BEL-7404 miR4458HG-knockout cells with the overexpression of SLC2A1 and HK2. **H** ECAR was detected in BEL-7404 WT and miR4458HG-knockout cells with the overexpression of SLC2A1 and HK2. **I** The relative lactic acid level was examined in SMMC-7721 cells co-transfected with control and SLC2A1 siRNA/HK2 siRNA or co-transfected with pcDNA3.1-miR4458HG and SLC2A1 siRNA/HK2 siRNA. **J** ECAR was detected in SMMC-7721 cells with control, pcDNA3.1-miR4458HG, and SLC2A1 siRNA transfection. **K** ECAR was detected in SMMC-7721 cells with control, pcDNA3.1-miR4458HG, and HK2 siRNA transfection

miR4458HG acted as an oncogenic lncRNA among patients with HCC

To investigate whether miR4458HG plays an essential role in HCC tumor progression in an unbiased manner, GSEA analysis was performed using TCGA RNA sequencing data (TCGA LIHC, $n=419$). Results showed that a high miR4458HG expression was associated with the gene signatures related to glycolysis and proliferation pathways (Fig. 2A, B). Furthermore, miR4458HG expression was positively correlated to glycolysis-related genes, including ENO1, ALDOA, and G6PD in TCGA database (Fig. S2A). These findings indicated that miR4458HG played an important catalytic role in HCC and glycolysis.

To evaluate the bioinformatics findings, miR4458HG siRNAs were purposefully introduced into the HCC cells, BEL-7404 and Hep3B. Higher levels of miR4458HG were obtained in BEL-7404 and Hep3B cells (Fig. S2B). miR4458HG knockdown markedly inhibited HCC cell proliferation in vitro (Fig. 2C–H, Fig. S2C-D) and suppressed BEL-7404 tumor volume (Figs. 2I, J, S2E) and tumor weight (Fig. 2K) in vivo. Ki67 staining revealed that miR4458HG knockdown effectively inhibited the in vivo multiplication of the tumor cells (Fig. S2F). In addition, SMMC-7721 and Huh7 cells with lower levels of miR4458HG demonstrated that cell proliferation was enhanced after miR4458HG overexpression in vitro (Figs. 2L, M, S2G–H). Our findings indicated that miR4458HG could enhance HCC tumor growth by modulating HCC cell multiplication.

miR4458HG influenced HCC cell survival by activating glycolysis pathway

Next, the ECAR was measured to determine the direct impact of the change in miR4458HG level on the glycolytic metabolism of HCC cells [16]. Indeed, compared with control cells with control siRNA transfection, miR4458HG knockdown markedly decreased ECAR in BEL-7404 and Hep3B cells (Fig. 3A, B). Colorimetric assay showed that miR4458HG downregulation markedly reduced the production of lactic acid in BEL-7404 and Hep3B cells (Fig. 3C, D). However, miR4458HG overexpression significantly enhanced ECAR (Fig. 3E, F) and lactic acid production (Fig. 3G, H) in SMMC-7721 and Huh7 cells. Importantly, miR4458HG induced increases in cell multiplication and lactic acid production in SMMC-7721 (Figs. 3I, S3A), and Huh7 cells were remarkably blocked by 2-deoxy-D-glucose (2-DG), which is a suppressor of glycolysis pathway (Fig. 3J, Fig. S3B). Furthermore, miR4458HG expression increased upon glucose starvation in SMMC-7721 cells (Fig. S3C). These results suggested that miR4458HG could be upregulated by glucose deprivation and further modulate glycolysis in HCC.

miR4458HG interacted with IGF2BP2 and modulated the mRNA stability of HK2 and SLC2A1 depending on RNA m6A modification

The miR4458HG expression in the nuclear and cytoplasm fractions was performed by qRT-PCR in HCC Hep3B cells. MiR4458HG was predominant in the cytoplasm (Fig. S4A). To analyze the mechanism of this lncRNA in tumorigenesis, the SILAC-based proteomic method [17, 18] combined with RNA pull-down assay was conducted to screen the proteins that interacted with miR4458HG (Fig. 4A). Among the specific interactors of sense miR4458HG (log2(H/L ratio) > 1) (Fig. 4B), the top five potential miR4458HG-binding proteins were selected for further binding validation. Based on the results of the RNA pull-down analysis, IGF2BP2 was the only protein binding to miR4458HG (Figs. 4C, S4B). These findings indicated that IGF2BP2 might interact with miR4458HG. IGF2BP2 is an m6A reader protein, which is important for the stability and function of many RNAs with m6A modifications, and further regulates important biological functions, including glycolysis and carcinogenesis [19]. To identify the exact location of the IGF2BP2-interacting region of miR4458HG, we developed and biotinylated six segments of miR4458HG (F1 denotes complete length of anti-sense miR4458HG, F2 denotes complete length of sense miR4458HG, F3: 1–1300 nt, F4: 1–850 nt, F5: 1–431 nt,

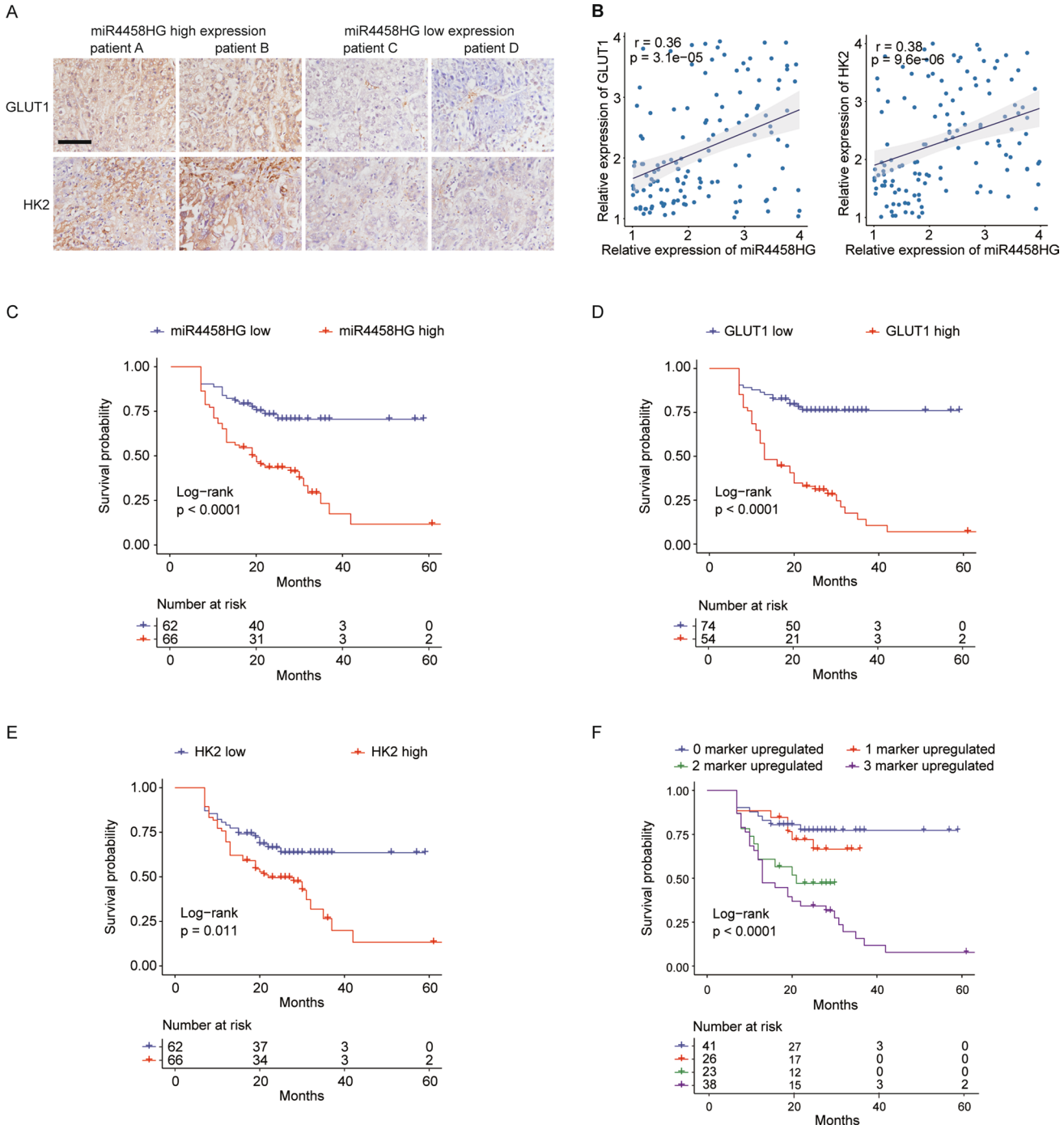

Fig. 6 The levels of miR4458HG and glycolysis components correlate and are clinically relevant in HCC patients. **A** The representative images of ISH of miR4458HG and immunohistochemical staining of GLUT1 and HK2 in cohort 2. Scale bar, 100 μm. **B** Correlation analysis between miR4458HG expression and GLUT1 IHC scores (left) and between miR4458HG expression and HK2 (right) in HCC tissues of cohort 2 ($n = 128$). **C** Longevity was examined and associated among subjects with higher and lower miR4458HG expression levels in the tumor in cohort 2; $n = 128$, log-rank test. **D** Longevity was examined and associated among subjects with higher and lower miR4458HG expression levels in the tumor in cohort 2; $n = 128$, log-rank test. **E** Longevity was examined and associated among subjects with higher and lower miR4458HG expression level in the tumor in cohort 2; $n = 128$, log-rank test. **F** Longevity was analyzed among HCC subjects based on the number of upregulated molecular markers (miR4458HG, GLUT1, and HK2) in cohort 2

F6: 432–1731 nt), and then subjected to pull-down analysis along with BEL-7404 cell lysates. Western blot assay showed that the 5' terminal of miR4458HG was essential for this lncRNA to interact with IGF2BP2 protein (Fig. 4D). To validate the results, RIP assay was performed by qRT-PCR and confirmed the interaction between miR4458HG and IGF2BP2 in HCC cells (Fig. 4E).

IGF2BP2 functions as an m6A RNA reader and stabilizes the m6A modification of target RNA in different biological physiological processes and tumor signaling pathways. This RNA m6A reader can also modify the m6A and mRNA level of HK2 and SLC2A1, which are the key components of glycolysis pathway in cancer biology [20]. Thus, we hypothesized that miR4458HG was responsible for IGF2BP2-mediated HK2 and SLC2A1 RNA stability depending on the RNA m6A modification. RIP followed by qRT-PCR assay demonstrated that miR4458HG downregulation significantly suppressed the binding between IGF2BP2 and the mRNA of HK2 or SLC2A1 in BEL-7404 (Fig. 4F) and Hep3B cells (Fig. 4G). The half-life of SLC2A1 and HK2 mRNA was markedly diminished in BEL-7404 cells (Fig. 4H) and Hep3B cells (Fig. 4I) after transfection with miR4458HG siRNA. Furthermore, knockdown of miR4458HG substantially reduced the RNA level of SLC2A1 and HK2 in BEL-7404 cells (Fig. 4J) and Hep3B cells (Fig. 4K). In addition, overexpression of miR4458HG significantly increased the HK2 and SLC2A1 expression, while knockdown of IGF2BP2 impaired the miR4458HG-induced upregulation of HK2 and SLC2A1 in SMMC-7721 cells (Figs. 4L, M, S5). In brief, these results indicated that miR4458HG might directly bound with IGF2BP2 and further regulate the m6A modification and the mRNA stability of SLC2A1 and HK2 in HCC cells.

HK2 and GLUT1 mediated the biological function of miR4458HG in HCC

Hexokinase 2 (HK2) is an essential kinase in glycolysis and participates in different carcinogenesis, including HCC [21]. SLC2A1 encodes GLUT1 (glucose transporter 1), a key glycolytic transporter, is also specifically expressed in HCC [22]. To the best of our knowledge, our study was able to demonstrate for the first time that miR4458HG promoted SLC2A1 and HK2 expression by increasing their mRNA stability. Consequently, rescue experiments were performed to examine the involvement of SLC2A1 and HK2 in the effects of miR4458HG in HCC. The SLC2A1, HK2, or control overexpression plasmid was transfected into the BEL-7404 with or without miR4458HG knockout (Fig. S6A, B). miR4458HG knockout remarkably inhibited BEL-7404 cell proliferation (Fig. 5A), colony formation (Fig. 5B, C), and tumor growth (Fig. 5D–F), which was partially restored by HK2 or SLC2A1 overexpression. Meanwhile, HK2 or SLC2A1 siRNA was transfected into the SMMC-7721 cells with miR4458HG overexpression plasmid or empty vector transfection (Fig. S6C, D). miR4458HG overexpression-induced cell proliferation (Fig. S6E) and colonization (Fig. S6F, G) were markedly rescued via downregulating of HK2 or SLC2A1. This data subsequently supported HK2 and SLC2A1 as important target genes of miR4458HG in HCC.

In glycolytic assays, the ectopic expression of HK2 or SLC2A1 reversed the reduction of lactate formation and glucose consumption, respectively, in BEL-7404 miR4458HG-knockout cells (Fig. 5G, H). Furthermore, HK2 or SLC2A1 downregulation significantly inhibited the miR4458HG-induced increase in lactate production (Fig. 5I) and glucose uptake (Fig. 5J, K) in SMMC-7721 cells. Therefore, SLC2A1 and HK2 participated in the biological function of miR4458HG in HCC cells.

miR4458HG and glycolysis components are pertinent clinically in patients with HCC

Immunohistochemical staining was performed on the tissues of patients in the hospital cohort 2. IHC data showed that strong staining of GLUT1 and HK2 was found in HCC patients with increased miR4458HG expression and vice versa (Fig. 6A), with statistical significance (Fig. 6B). Moreover, the miR4458HG expression was positively correlated to the protein level of HK2 and GLUT1 in HCC tissues. Subsequently, the strength of miR4458HG, glycolytic constituent, and overall longevity were further analyzed. Survival analysis revealed higher expression of miR4458HG, GLUT1 or HK2 predicted robustly shorter clinical outcome in HCC participants of cohort 2 (Fig. 6C–E). Patients with three highly expressed markers showed the shortest overall survival time (Fig. 6F). Thus, a higher miR4458HG, GLUT1, and HK2 expression might indicate poor prognosis in HCC patients.

Exosomal miR4458HG promoted tumor-associated macrophage polarization and induces tumor progression

Results of the correlation analysis showed that the miR4458HG expression was positively correlated to the CD68 and ARG1 expression in macrophage cells (Fig. 7A), indicating that miR4458HG might mediate the function of tumor-associated macrophage cells. We next hypothesized that miR4458HG was wrapped in the exosomes, which was secreted from HCC cells and further entered the macrophage cells to perform its biological function. qRT-PCR data showed that the exosomes of miR4458HG were significantly increased in different HCC cells, compared with those of LO2 hepatocytes (Fig. S7A). In addition, a high exosomal miR4458HG level was detected in Hep3B HCC

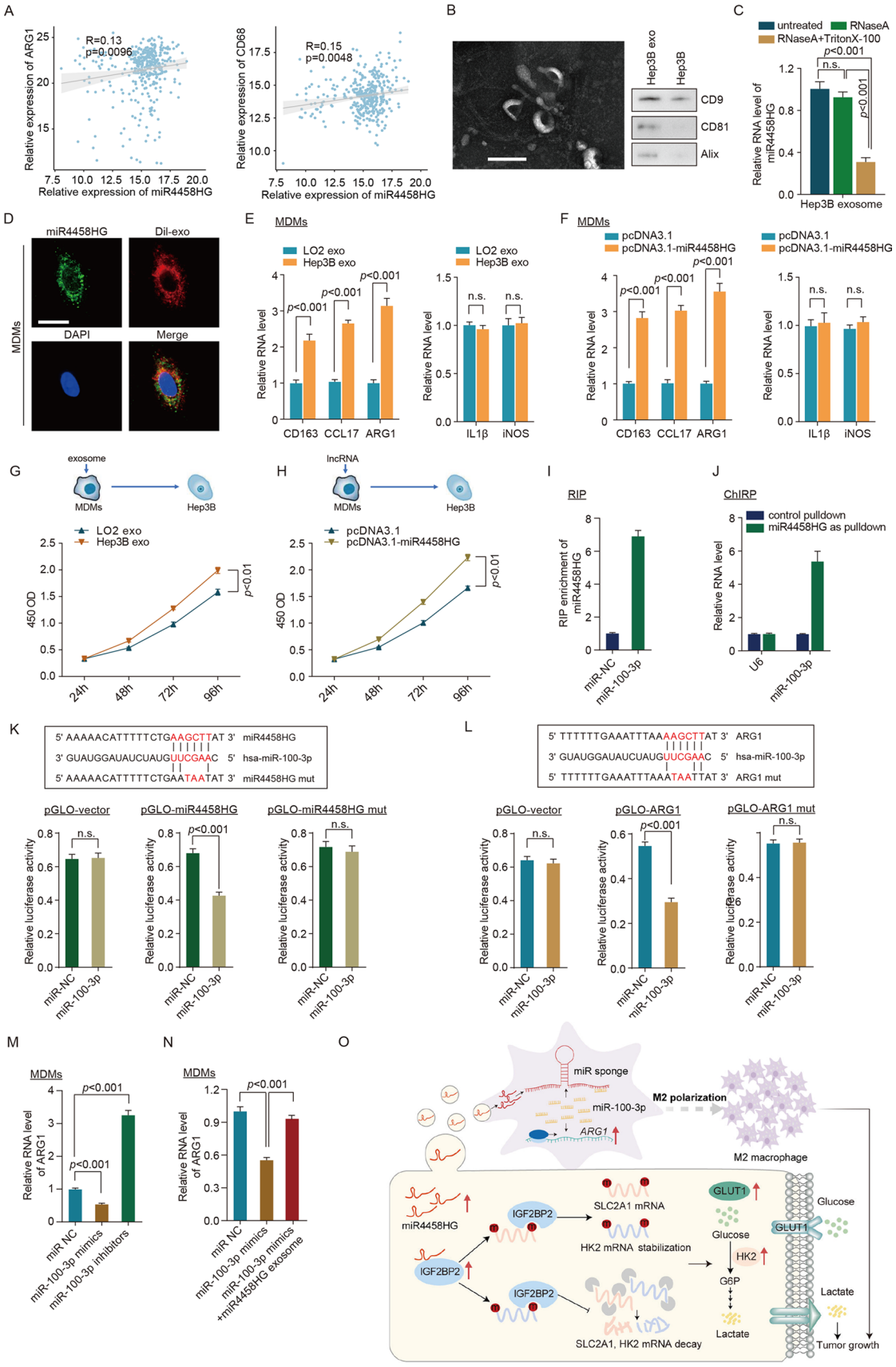
A
Relative expression of ARG1
R=0.13
p=0.0096
Relative expression of miR4458HG
Relative expression of CD68
R=0.15
p=0.0048
Relative expression of miR4458HG
B
Hep3B exo
Hep3B
CD9
CD81
Alix
C
untreated
RNaseA
RNaseA+TritonX-100
p<0.001
n.s.
p<0.001
Relative RNA level of miR4458HG
Hep3B exosome
D
miR4458HG
Dil-exo
DAPI
Merge
MDMs
E
MDMs
LO2 exo
Hep3B exo
p<0.001
Relative RNA level
CD163 CCL17 ARG1
n.s.
IL1β iNOS
F
MDMs
pcDNA3.1
pcDNA3.1-miR4458HG
p<0.001
Relative RNA level
CD163 CCL17 ARG1
n.s.
IL1β iNOS
G
exosome
MDMs
Hep3B
LO2 exo
Hep3B exo
450 OD
p<0.01
24h 48h 72h 96h
H
lncRNA
MDMs
Hep3B
pcDNA3.1
pcDNA3.1-miR4458HG
450 OD
p<0.01
24h 48h 72h 96h
I
RIP
RIP enrichment of miR4458HG
miR-NC
miR-100-3p
J
ChIRP
control pulldown
miR4458HG as pulldown
Relative RNA level
U6
miR-100-3p
K
5' AAAAACATTTTTCTGAAGCTTAT 3' miR4458HG
3' GUAUGGAUAUCUAUGUUCGAAC 5' hsa-miR-100-3p
5' AAAAACATTTTTCTGAATAATAT 3' miR4458HG mut
pGLO-vector
pGLO-miR4458HG
pGLO-miR4458HG mut
n.s.
p<0.001
n.s.
Relative luciferase activity
miR-NC
miR-100-3p
L
5' TTTTTTGAAATTTAAAAGCTTAT 3' ARG1
3' GUAUGGAUAUCUAUGUUCGAAC 5' hsa-miR-100-3p
5' TTTTTTGAAATTTAAATAATTAT 3' ARG1 mut
pGLO-vector
pGLO-ARG1
pGLO-ARG1 mut
n.s.
p<0.001
n.s.
Relative luciferase activity
miR-NC
miR-100-3p
M
MDMs
p<0.001
p<0.001
Relative RNA level of ARG1
miR NC
miR-100-3p mimics
miR-100-3p inhibitors
N
MDMs
p<0.001
Relative RNA level of ARG1
miR NC
miR-100-3p mimics
miR-100-3p mimics +miR4458HG exosome
O
miR sponge
miR-100-3p
ARG1
M2 polarization
M2 macrophage
miR4458HG
IGF2BP2
SLC2A1 mRNA
HK2 mRNA stabilization
IGF2BP2
IGF2BP2
SLC2A1, HK2 mRNA decay
GLUT1
Glucose
Glucose
GLUT1
HK2
G6P
Lactate
Lactate
Tumor growth

◂**Fig. 7** Exosomal miR4458HG promotes tumor-associated macrophage polarization and induces tumor progression. **A** Correlation analysis between miR4458HG expression and ARG1 expression (left) in HCC tissues of cohort 2 ($n=128$). Correlation analysis between miR4458HG expression and CD68 expression (right) in the HCC tissues of cohort 2. **B** Electron microscope observation of the morphology of Hep3B exosomes. Western blot analysis of antigens (CD9, CD81, and Alix) in Hep3B exosomes (Hep3B exo). Scale bar, 200 nm. **C** qRT-PCR analysis of miR4458HG in the exosomes derived from Hep3B cells treated with RNase A alone or combined with Triton X-100. **D** Fluorescent staining was performed in MDMs after incubation with Dil-labeled (red) exosomes derived from Hep3B cells. Scale bar, 20 μm. **E** The expression level of M2 macrophages markers (CD163, CCL17, and ARG1) and M1 macrophages markers (IL-1β and iNOS) in MDMs treated with exosome extracted from LO2 cells (normal hepatocytes) or Hep3B cells as indicated. **F** The expression level of M2 macrophages markers (CD163, CCL17, and ARG1) and M1 macrophage markers (IL-1β and iNOS) in MDMs with miR4458HG overexpression. **G** Hep3B cells cultured with MDMs treated with exosome extracted from LO2 or Hep3B cells for 48 h in Transwell systems for 10 days, and then Hep3B cells were collected for cell proliferation. **H** Hep3B cells were co-cultured with MDMs-control and MDMs-miR4458HG in Transwell systems for 10 days and then collected for cell proliferation. **I** Anti-AGO2 RIP was conducted in MDMs with transient transfection of miR-100-3p and miR-NC, and qRT-PCR was performed to identify miR4458HG associated with AGO2. **J** ChIRP followed by qRT-PCR to detect miR-100-3p that endogenously related with miR4458HG. U6 was used as a negative control. **K** Sequence alignment of miR-100-3p with miR4458HG and miR4458HG mutant (top). Dual-luciferase reporter assays of pGLO-vector, pGLO-miR4458HG, and pGLO-miR4458HG mutant (pGLO-miR4458HG mut) (bottom). **L** Sequence alignment of miR-100-3p with ARG1 and ARG1 mutant (top). Dual-luciferase reporter assays of pGLO-vector, pGLO-ARG1, and pGLO-ARG1 mutant (pGLO-ARG1 mut) (bottom). **M** The RNA level of ARG1 was detected in MDMs treated with the indicated microRNA mimics or inhibitors of miR-100-3p. **N** The RNA level of ARG1 was detected in MDMs treated with the microRNA mimics of miR-100-3p and miR4458HG as indicated. **O** Schematic diagram for the mechanism showing that miR4458HG/IGF2BP2 regulates glycolysis metabolism in HCC cancer development by stabilizing the transcription of SLC2A1 and HK2

cells with more cellular miR4458HG, compared with LO2 hepatocytes (Fig. S7B). Furthermore, the exosomes were isolated from HCC Hep3B cells by centrifugation. Electromicroscopy data showed the presence of Hep3B exosomes (Hep3B-exo) with a diameter of 40–140 nm (Fig. 7B). In addition, Western blot analysis further showed that exosome markers CD9, CD81, and Alix were identified in Hep3B-exo (Fig. 7B). qRT-PCR also showed that the miR4458HG expression level was significantly downregulated in Hep3B-exo in response to RNase A and Triton X-100 simultaneous treatment, but not significantly altered upon RNase A treatment alone (Fig. 7C), indicating that extracellular miR4458HG was mainly wrapped in the exosomes. In confocal immunofluorescent assay, co-localization of FAM-labeled miR4458HG (green) and Dil-labeled exosomes (red) was observed in the human monocyte-derived macrophages (MDMs) cells after exosome incubation, indicating that the exosomes-mediated miR4458HG transferring could occur between the macrophage and Hep3B cells (Fig. 7D).

To investigate the role of miR4458HG in tumor-associated macrophage polarization, the expression of immunoactivating macrophages (M1) markers and immunosuppressive macrophages (M2) markers in human MDMs was evaluated. qRT-PCR data showed that M2 markers of the macrophage, but not M1 markers, were significantly increased in MDMs cells after inoculation with Hep3B exosomes with a higher level of miR4458HG (Fig. 7E). In addition, the overexpression of miR4458HG significantly increased the expression of M2 markers of the macrophage in MDMs cells (Fig. 7F). To explore the role of human MDMs with a higher miR4458HG expression in the regulation of HCC tumor cell growth, Hep3B-derived exosomes were first incubated with human MDMs (exo-MDMs) or transfected pCDNA3.1-miR4458HG into MDMs. These exo-MDMs and MDMs with a higher expression of miR4458HG (miR4458HG-MDMs) were then respectively co-cultured with Hep3B cells in a Transwell system, whereby the exo-MDMs and miR4458HG-MDMs were not physically interacting with the HCC cells. After 10 days of inoculation, the Hep3B cells co-cultured with exo-MDMs or miR4458HG-MDMs exhibited a higher level of cell proliferation (Fig. 7G, H) compared with control cells. In clinical validation assay, qRT-PCR was performed and confirmed the existence of exosomal miR4458HG in the serum sample of HCC patients (Fig. S7C). In addition, according to the expression level of exosomal miR4458HG in the serum, HCC patients were divided into high- and low-expression groups, respectively. qRT-PCR assay showed the presence of higher levels of CD163, CCL17, and ARG1 in tissue-isolated macrophages of HCC patients with high miR4458HG expression (Fig. S7D–F). These data indicated that miR4458HG might mediate the polarization of tumor-associated macrophage.

Next, we explored the potential mechanism of exo-miR4458HG in macrophage polarization. The exosome-wrapped lncRNA usually acts as a ceRNA to perform its biological function [23, 24]. Therefore, we next used bioinformatical analysis tools (Eran Segal; http://132.77.150.113/pubs/mir07/mir07_prediction.html) to predict the potential target miRNA of miR4458HG. The analysis data showed that miR-100-3p is the potential candidate to bind miR4458HG. To verify the binding between miR-100-3p and miR4458HG, RIP assay was performed with anti-AGO2 antibody in MDMs. The data confirmed the involvement of miR4458HG and miR-100-3p in the RISC of MDMs (Fig. 7I). Further, ChIRP validation assay showed that miR4458HG could directly interact with miR-100-3 in MDMs (Figs. 7J, S7G). In addition, pGLO-miR4458HG was constructed with the full-length of miR4458HG in a luciferase reporter plasmid. miR-100-3p overexpression significantly downregulated the luciferase activity of the

miR4458HG reporter plasmid, but not the control plasmid (Fig. 7K), and the pGLO-miR4458HG-mut with miR-100-3p binding site mutation. Next, the target genes of miR-100-3p and miR4458HG were predicted by Targetscan (http://www.targetscan.org/). After bioinformatical analysis, we selected, for further validation, ARG1, which plays important roles in polarization of macrophage cells. Luciferase assays were performed, and the data showed that the luciferase activity was significantly reduced after transfection of miR-100-3p mimics in MDMs cells with ARG1 reporter plasmid transfection, but not the mutated plasmid (Fig. 7L). Next, qRT-PCR (Fig. 7M) demonstrated that ARG1 expression was reduced by miR-100-3p mimics and increased by miR-100-3p inhibitors. Furthermore, miR4458HG overexpression significantly blocked the miR-100-3p-induced downregulation of ARG1 in MDMs (Fig. 7N). These data indicated that ARG1 was the direct target of miR-100-3p in MDMs cells, and miR4458HG-mediated macrophage polarization depended on blocking the miR-100-3p-mediated ARG1 downregulation.

Discussion

Numerous oncogenic signal pathways may contribute to HCC [25]. However, the influence of lncRNAs in the arrangement of glucose metabolism and in human HCC is poorly defined. Based on the results of genomic, biochemical, and functional analysis, we proved that miR4458HG is a carcinogenic lncRNA in HCC and associated with cell proliferation and glycolytic pathways. In in vitro and in vivo experimental models, miR4458HG downregulation significantly inhibits cell proliferation and glycolysis activation in HCC, suggesting that a high miR4458HG expression is essential to regulate human HCC malignancy.

The biological functions of lncRNAs usually depend on their subcellular localizations [26]. The nuclear lncRNAs regulate the transcription or post-transcriptional modification of target genes and further influence different signal transduction pathways [26]. Yet, the mechanism by which the disease progress starts remains unexplored particularly in HCC. In this study, LC–MS combined with RNA pull-down assay showed that miR4458HG directly bound to the RNA m6A reader IGF2BP2 and further facilitated the m6A modification level and mRNA stability of target genes (HK2 and SLC2A1); subsequently, glycolytic metabolic reactions were initiated. The following findings in previous studies support these results: (i) miR4458HG directly interacted with IGF2BP2 via its 5′ domain; (ii) downregulation of miR4458HG abrogated the binding efficiency between IGF2BP2 and the mRNA region of SLC2A1 and HK2; (iii) the breakdown of miR4458HG effectively interferes with the m6A modification and RNA half-life level of the target genes of IGF2BP2, SLC2A1 and HK2, which are the key components of glycolysis pathway; and (iv) miR4458HG, which could be wrapped in the exosome and secreted out by HCC cells, might act as an microRNA sponge, increase ARG1 expression, and further promote tumor-associated macrophage polarization (Fig. 7O). To the best of our knowledge, miR4458HG is the first lncRNA that can modulate the target RNA stability by enhancing the binding and the recognition efficiency of m6A reader IGF2BP2 to its target genes and by further altering the glycolytic metabolism and cancer biology function and tumor microenvironment in HCC tissue subunits.

On exploring the process by which miR4458HG enhances the HCC, it was clear that HK2s and SLC2A1 (GLUT1) play a role as important kinase in the glycolysis pathway [21]. A recent study demonstrated an increased activity of HK2 in HCC cells [27]. In addition, GLUT1 is the essential glucose transporter expressed in hepatic cells and the major regulator of glycolysis pathway [28]. In our study, we first showed that miR4458HG facilitates IGFBP2 to recognize and stabilize the mRNA level of SLC2A1 and HK2 dependent on m6A modification and then further increase the mRNA and protein scores of SLC2A1 and HK2. In addition, HK2 and SLC2A1 are involved in the miR4458HG-mediated glucose metabolism and tumorigenesis in HCC.

Previous studies have demonstrated the Warburg effect and its involvement in cell proliferation in several solid tumors including HCC [29]. In the present study, we found an increased miR4458HG expression upon glucose deprivation, which assisted in achieving IGF2BP2-mediated HK2 and SLC2A1 m6A RNA stability and promoted glycolysis in HCC cells. The abnormal activation of miR4458HG/IGFBP2/HK2/SLC2A1 glycolysis cascade might be the new glucose metabolism pattern for HCC to survive. Therefore, based on our results, miR4458HG was a potential key component for HCC glucose metabolism reprogramming. MiR4458HG, an oncogenic lncRNA, is sufficient in moderating the m6A modification pattern of IGF2BP2 and further stabilizing SLC2A1 and HK2 mRNA and regulating glycolysis in HCC cells.

In addition, the present study revealed that HCC cells may produce exosomes to transmit miR4458HG to macrophage cells and further promote the polarization of tumor-associated macrophage cells. Exosomes is composed of a larger number of non-coding RNAs, including microRNAs and lncRNAs. Exosome-wrapped non-coding RNAs could be effectively delivered into target cells to regulate their biological functions [30, 31]. Here, miR4458HG, an HCC cell-derived lncRNA, is released via exosomes from the HCC cells to the macrophage cells to act as miR-100-3p sponge and further stabilize the mRNA stability of ARG1, which is the major marker of tumor-associated macrophage. This shows that miR4458HG

lncRNA could mediate the communication between macrophage and HCC cells, and further promote the generation of the immunosuppressive microenvironment in HCC.

Given the essential and pivotal role of miR4458HG in HCC, we concluded that miR4458HG enhanced the HCC tumor growth and glycolysis in vitro and in vivo by directly interacting with IGF2PB2 to stabilize the mRNA level of SLC2A1 and HK2, subsequently enhancing the HCC progression and glycolysis pathway. Thus, miR4458HG and its associated pathway may be potential tools to identify prognostic biomarkers and therapeutic targets among patients with HCC.

Supplementary Information The online version contains supplementary material available at https://doi.org/10.1007/s00018-023-04741-8.

Author contributions YY: conceptualization (equal); writing—original draft (equal). MW: investigation (equal); methodology (equal). GW: data curation (equal); software (equal). ZM: methodology (equal); validation (equal). BZ: investigation (equal); visualization (equal). YH: methodology (equal); data curation (equal); visualization (equal). JZ: software (equal); validation (equal). WX: conceptualization (equal); writing—review and editing (lead). All the authors read and approved the final manuscript.

Funding This work was supported by National Natural Science Foundation of China (81873178, 81904036), The leading talent Training Program of Pudong Health Burea of Shanghai (PWRl2019-03), Excellent subject leader training project of the three-year action plan of Shanghai public health system (GWV-10.2-XD15), and Key discipline construction project of the three-year action plan of Shanghai public health system (GWV-10.1-XK9).

Data availability The dataset generated and/or analyzed during the current study are available from the corresponding author on reasonable request.

Declarations

Conflict of interest No potential conflicts of interest were disclosed.

Ethics approval Animal experiments were carried out in accordance with the standards approved by the Ethics Committee of The Seventh People's Hospital of Shanghai University of Traditional Chinese Medicine.

Consent to participate The use of samples from patients was conducted according to the guidelines of the Declaration of Helsinki and approved by the Ethics Committee of The Seventh People's Hospital of Shanghai University of Traditional Chinese Medicine. The need to obtain informed consent from the study patients was waived.

Consent to publish Not applicable.

References

1. Gores GJ (2014) Decade in review-hepatocellular carcinoma: HCC-subtypes, stratification and sorafenib. Nat Rev Gastroenterol Hepatol 11(11):645–647
2. Wang X, Zhang A, Sun H (2013) Power of metabolomics in diagnosis and biomarker discovery of hepatocellular carcinoma. Hepatology 57(5):2072–2077
3. Moawad AW, Szklaruk J, Lall C et al (2020) Angiogenesis in hepatocellular carcinoma; pathophysiology, targeted therapy, and role of imaging. J Hepatocell Carcinoma 7:77–89
4. Koppenol WH, Bounds PL, Dang CV (2011) Otto Warburg's contributions to current concepts of cancer metabolism. Nat Rev Cancer 11(5):325–337
5. Hsu PP, Sabatini DM (2008) Cancer cell metabolism: Warburg and beyond. Cell 134(5):703–707
6. Wong TL, Ng KY, Tan KV et al (2020) CRAF methylation by PRMT6 regulates aerobic glycolysis-driven hepatocarcinogenesis via ERK-dependent PKM2 nuclear relocalization and activation. Hepatology 71(4):1279–1296
7. Zuo Q, He J, Zhang S et al (2021) PPARgamma coactivator-1alpha suppresses metastasis of hepatocellular carcinoma by inhibiting Warburg effect by PPARgamma-dependent WNT/beta-catenin/pyruvate dehydrogenase kinase isozyme 1 axis. Hepatology 73(2):644–660
8. Necsulea A, Soumillon M, Warnefors M et al (2014) The evolution of lncRNA repertoires and expression patterns in tetrapods. Nature 505(7485):635–640
9. Marin-Bejar O, Mas AM, Gonzalez J et al (2017) The human lncRNA LINC-PINT inhibits tumor cell invasion through a highly conserved sequence element. Genome Biol 18(1):202
10. Schmitt AM, Chang HY (2016) Long noncoding RNAs in cancer pathways. Cancer Cell 29(4):452–463
11. Brauze D, Mikstacka R, Pelkonen O (1990) Monoclonal antibody characterization of NADH- and NADPH-dependent hydroxylation of benzo(a)pyrene in liver microsomes from 5,6-benzoflavone-induced C57Bl/6 mice. Acta Biochim Pol 37(2):219–225
12. Gupta RA, Shah N, Wang KC et al (2010) Long non-coding RNA HOTAIR reprograms chromatin state to promote cancer metastasis. Nature 464(7291):1071–1076
13. Shen C, Xuan B, Yan T et al (2020) m(6)A-dependent glycolysis enhances colorectal cancer progression. Mol Cancer 19(1):72
14. Cox J, Mann M (2008) MaxQuant enables high peptide identification rates, individualized ppb-range mass accuracies and proteome-wide protein quantification. Nat Biotechnol 26(12):1367–1372
15. Lu Y, Yang A, Quan C et al (2022) A single-cell atlas of the multicellular ecosystem of primary and metastatic hepatocellular carcinoma. Nat Commun 13(1):4594
16. Zhang J, Nuebel E, Wisidagama DR et al (2012) Measuring energy metabolism in cultured cells, including human pluripotent stem cells and differentiated cells. Nat Protoc 7(6):1068–1085
17. Ong SE, Blagoev B, Kratchmarova I et al (2002) Stable isotope labeling by amino acids in cell culture, SILAC, as a simple and accurate approach to expression proteomics. Mol Cell Proteomics 1(5):376–386
18. Wang T, Gu S, Ronni T, Du YC, Chen X (2005) In vivo dual-tagging proteomic approach in studying signaling pathways in immune response. J Proteome Res 4(3):941–949
19. Huang H, Weng H, Sun W et al (2018) Recognition of RNA N(6)-methyladenosine by IGF2BP proteins enhances mRNA stability and translation. Nat Cell Biol 20(3):285–295
20. Wang Y, Lu JH, Wu QN et al (2019) LncRNA LINRIS stabilizes IGF2BP2 and promotes the aerobic glycolysis in colorectal cancer. Mol Cancer 18(1):174
21. Patra KC, Wang Q, Bhaskar PT et al (2013) Hexokinase 2 is required for tumor initiation and maintenance and its systemic deletion is therapeutic in mouse models of cancer. Cancer Cell 24(2):213–228
22. Kawai T, Yasuchika K, Seo S et al (2017) Identification of keratin 19-positive cancer stem cells associating human hepatocellular

carcinoma using (18)F-fluorodeoxyglucose positron emission tomography. Clin Cancer Res 23(6):1450–1460
23. Chen X, Wang Z, Tong F, Dong X, Wu G, Zhang R (2020) lncRNA UCA1 promotes gefitinib resistance as a ceRNA to target FOSL2 by sponging miR-143 in non-small cell lung cancer. Mol Ther Nucleic Acids 19:643–653
24. Wu XS, Wang F, Li HF et al (2017) LncRNA-PAGBC acts as a microRNA sponge and promotes gallbladder tumorigenesis. EMBO Rep 18(10):1837–1853
25. Li X, Li C, Zhang L et al (2020) The significance of exosomes in the development and treatment of hepatocellular carcinoma. Mol Cancer 19(1):1
26. Chen LL (2016) Linking long noncoding RNA localization and function. Trends Biochem Sci 41(9):761–772
27. DeWaal D, Nogueira V, Terry AR et al (2018) Hexokinase-2 depletion inhibits glycolysis and induces oxidative phosphorylation in hepatocellular carcinoma and sensitizes to metformin. Nat Commun 9(1):446
28. Amann T, Maegdefrau U, Hartmann A et al (2009) GLUT1 expression is increased in hepatocellular carcinoma and promotes tumorigenesis. Am J Pathol 174(4):1544–1552
29. Iansante V, Choy PM, Fung SW et al (2015) PARP14 promotes the Warburg effect in hepatocellular carcinoma by inhibiting JNK1-dependent PKM2 phosphorylation and activation. Nat Commun 6:7882
30. Melo SA, Sugimoto H, O'Connell JT et al (2014) Cancer exosomes perform cell-independent microRNA biogenesis and promote tumorigenesis. Cancer Cell 26(5):707–721
31. Zhou W, Fong MY, Min Y et al (2014) Cancer-secreted miR-105 destroys vascular endothelial barriers to promote metastasis. Cancer Cell 25(4):501–515